Satellite Droplet Formation in a Liquid Jet

Abstract: The formation and behavior of satellite droplets in a liquid jet is investigated experimentally and theoretically. The satellite droplet break-off distance is measured stroboscopically as a function of the frequency and amplitude of nozzle vibration. A second-order analysis of spatial instability is developed, which demonstrates the essential features of satellite formation as it is observed. Satellite formation is least likely to occur when the main-drop spacing is five to seven times the jet diameter.

Introduction

A liquid jet emanating from a nozzle, excited by a small-amplitude axial vibration of appropriate frequency, breaks up into uniformly spaced drops. Such a jet, however, also has a propensity to produce relatively small satellite droplets interspersed among the main drops. The existence and behavior of these satellites depend upon conditions of the jet. Satellite separation from a main drop can occur on the fore side of the droplet first, on the aft side first, or on both ends simultaneously. In this latter case, no momentum transfer takes place between the two main drops and the satellite—the interaction time is zero. This is the so-called "infinite" satellite condition and it is quite reproducible experimentally.

There are, perhaps, some applications in which the existence of satellites in a liquid jet is of benefit. Printing with an ink jet is not one of them, however. Therefore, for that application, it is important to understand the conditions for occurrence of these satellites in order to learn how to suppress their formation. The relative wavelength, i.e., the spacing of the main drops relative to the initial jet diameter, and the amplitude of the perturbing excitation are the most important parameters, although the liquid properties and the jet velocity are also significant.

Existing theories of drop formation do not suffice to explain satellite formation. The linear analyses of Rayleigh [1, 2], Weber [3], Keller et al. [4], and Pimbley [5] do not predict the formation of satellite droplets at all. On the other hand, nonlinear theories using a temporal instability, such as those of Yuen [6] and, more recently, Lee [7], always predict the existence of satellites along with the main drops. Furthermore, those nonlinear theories always predict satellite separation from the main drops at both ends at the same time, and this prediction disagrees with experimental observations.

The principal effort of this paper is a nonlinear analysis through second order of the drop formation problem using a spatial instability. The one-dimensional model which has been used previously [5-7] is used again in this analysis. This model makes the problem tractable in that only nine eigenfunctions are required. Keller et al. [4] looked at the spatial instability problem using a three-dimensional model and encountered an infinity of eigenfunctions. The one-dimensional model requires the approximation that the wavelength (drop separation) be significantly greater than the radius of the jet stream. Lee [7] has shown that this approximation is valid in a linear analysis for jets with relatively large velocity. One must be cautious, however, in applying the model to higher order terms where shorter wavelengths are encountered.

Presented first in this paper are our experimental measurements and a discussion of our observations of the satellite condition. Next our spatial instability analysis is presented and applied to the separation point of the jet to consider satellite formation and behavior. Discussion and summary complete the paper.

Measurement and interpretation of satellite condition

Observations of drop formation from a liquid jet were made using five different jet-emitting assemblies. The nozzles were all made of glass and had, nominally, the same dimensions; the diameter was 63 μ m, and the length of the constant diameter section was 100 μ m. The assemblies were all vibrated magnetostrictively and although the mechanical structures of the assemblies varied, these latter characteristics are not important to our observations of the jet stream itself. Except for one set (G) of experiments in which distilled water was used, the liquid

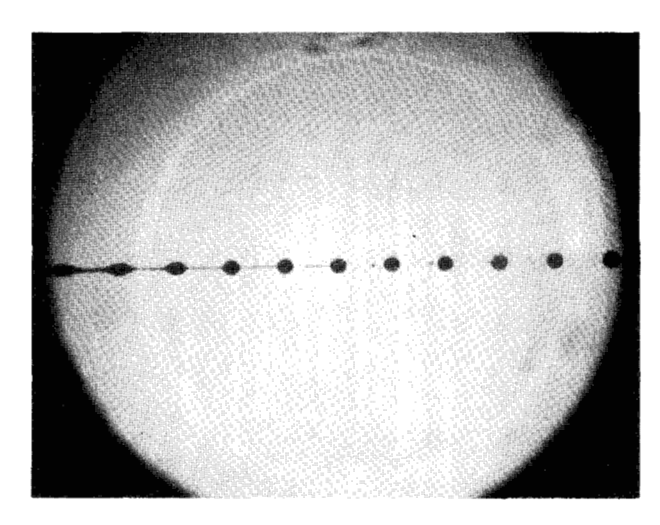


Figure 1 Stroboscopic microphotograph of a liquid jet showing forward-merging satellites. The nozzle diameter was 63 μ m, the jet velocity 9.0 m/s, and $\lambda/d = 5.3$.

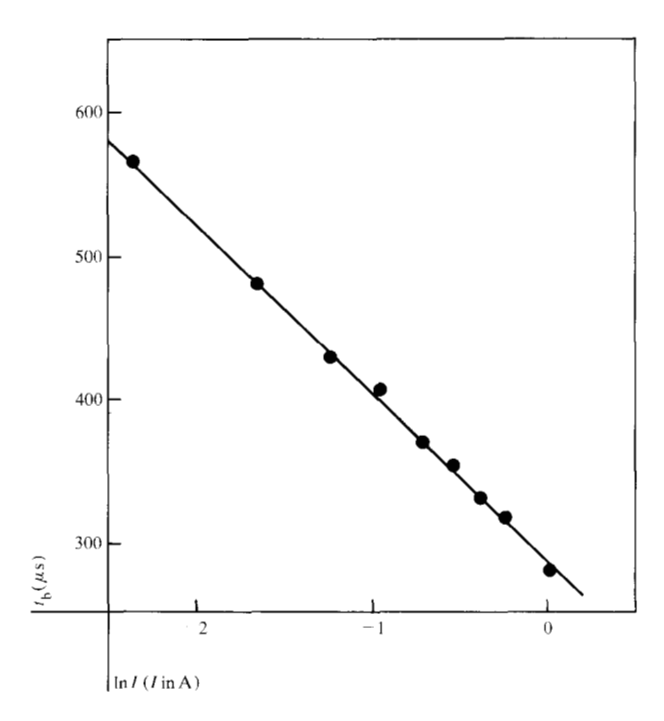


Figure 2 Data indicating linear operation of the jet-emitting assembly at f = 33 kHz and $\lambda/d = 5.1$.

was an ink with the following properties: surface tension, T=35 dynes/cm (0.035 N/m); density, $\rho=1.3 \text{ g/cm}^3 (1.3 \times 10^3 \text{ kg/m}^3)$; and viscosity, 8.7 centipoise (0.0087 Pa-s) as measured on a Ferranti-Shirley viscometer.

Experimental observations were made using a microscope (about 60×) with a cross-hair reticle with the

liquid jet being back-illuminated by a light-emitting diode strobed in synchronization with the jet excitation frequency. The entire jet-emitting assembly was mounted on an x-y table so that a micrometer with calibration to 0.0001 inch (0.0025 mm) could be used to measure distance along the jet. The wavelength was obtained by measuring the distances between the first ten drops after drop separation. Also, the drop separation distance was measured. These data, together with the excitation frequency as measured by an electronic counter, permitted us to calculate the jet velocity and then the break-off time.

The satellite condition was recorded by first noting the presence or absence of satellite separation and then, if separation had occurred, the distance downstream at which the satellite merged with a main drop. Whether the satellite droplet merged forward with the parent drop previously emitted or backward with the next main drop was also noted. The infinite satellite condition occurs when the satellite moves with the same velocity as the main stream parent drops and no merging occurs. This condition is quite sharp and reproducible as compared with other merge conditions.

Figure 1 is a photograph of a typical liquid jet viewed through a stroboscopically illuminated microscope. Forward-merging satellites are formed which merge three wavelengths downstream from their point of formation.

The linear portion of Lee's analysis using a temporal instability [7] predicts the satellite break-off time quite well. The relation between $t_{\rm b}$ and the initial velocity perturbation Δv at the nozzle can be expressed as

$$e^{-\gamma t_{\rm b}} = \pi \Delta v / 2\lambda \gamma,\tag{1}$$

where γ is the Rayleigh instability factor. Equation (1) indicates a logarithmic dependence between the break-off time and the perturbation amplitude. If one assumes that the vibrating jet-emitting assembly is operated in the linear region so that the velocity perturbation amplitude is proportional to the exciting current amplitude, then the drop break-off time should be linearly dependent on the logarithm of the exciting current amplitude. Also, the slope of this linear relationship should yield the value of the Rayleigh instability factor for the particular situation. Figure 2 shows typical results from one set of data in which only the current amplitude was varied. If this amplitude is raised much above the values shown in this figure, an overdrive situation occurs in which the data depart from the straight line, i.e., from the linear region of operation.

Figure 3 shows the Rayleigh instability factors obtained from all of the data for one of the jet-emitting assemblies. The solid curve is the instability factor as predicted by Rayleigh's analysis [1] for an inviscid liquid. The dashed curve shows the prediction for a viscous

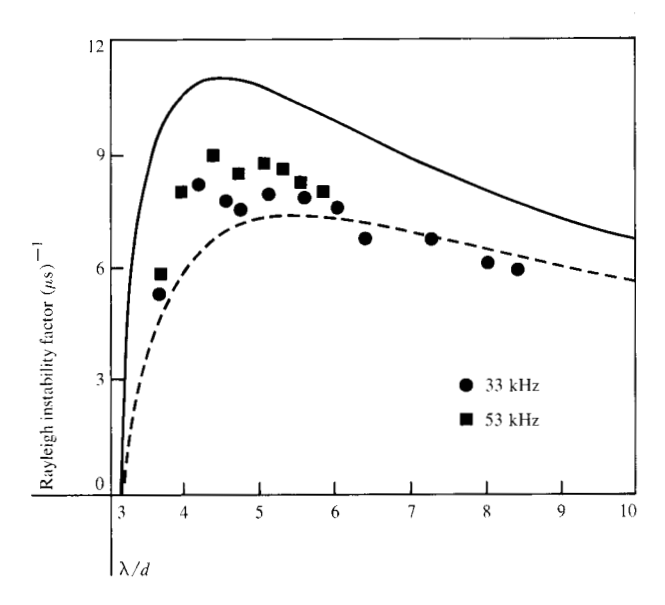


Figure 3 The Rayleigh instability factor as a function of f and λ/d . The solid curve is Rayleigh's theoretical result [1] for an inviscid liquid with parameters $T=0.035~\mathrm{N/m}$, $\rho=1.3~\mathrm{g/cm^3}$ (1300 kg/m³), and $a=30~\mu\mathrm{m}$. The dashed curve is Weber's theoretical result [3] for a liquid of viscosity 0.087 Pa-s.

Table 1 Straight-line* parameters for the infinity condition data shown in Figure 4.

Data set	Frequency (kHz)	Slope	Intercept
A	33	0.29	4.3
В	53	0.30	4.3
C	51	0.27	4.4
D	36	0.25	4.4
Е	40	0.30	4.1
F	34	0.28	4.4
G†	34	0.27	4.4

^{*} $\ln t_b = a(\lambda/d) + b$, t_b in μ s.

liquid given by Weber's analysis [3], the viscosity being 8.7 centipoise (0.0087 Pa-s) in this case. The data taken at a perturbation frequency of 53 kHz yield generally higher instability factors, and represent a higher jet velocity ($v = f\lambda$), than those at 33 kHz. This seems to indicate that the liquid is acting in a non-Newtonian manner—the higher velocities result in higher strain rates in the nozzle.

Figure 4 shows the loci of points for our observations of the infinity condition. Each point gives the break-off time at which the infinity condition occurred for a set of data in the experiments. Six runs were made with an ink and the seventh, G, with distilled water. Essentially all the data are superposable but each run has been plotted separately by uniformly shifting the linear ordinate scale. As can be seen, the data form straight lines when the

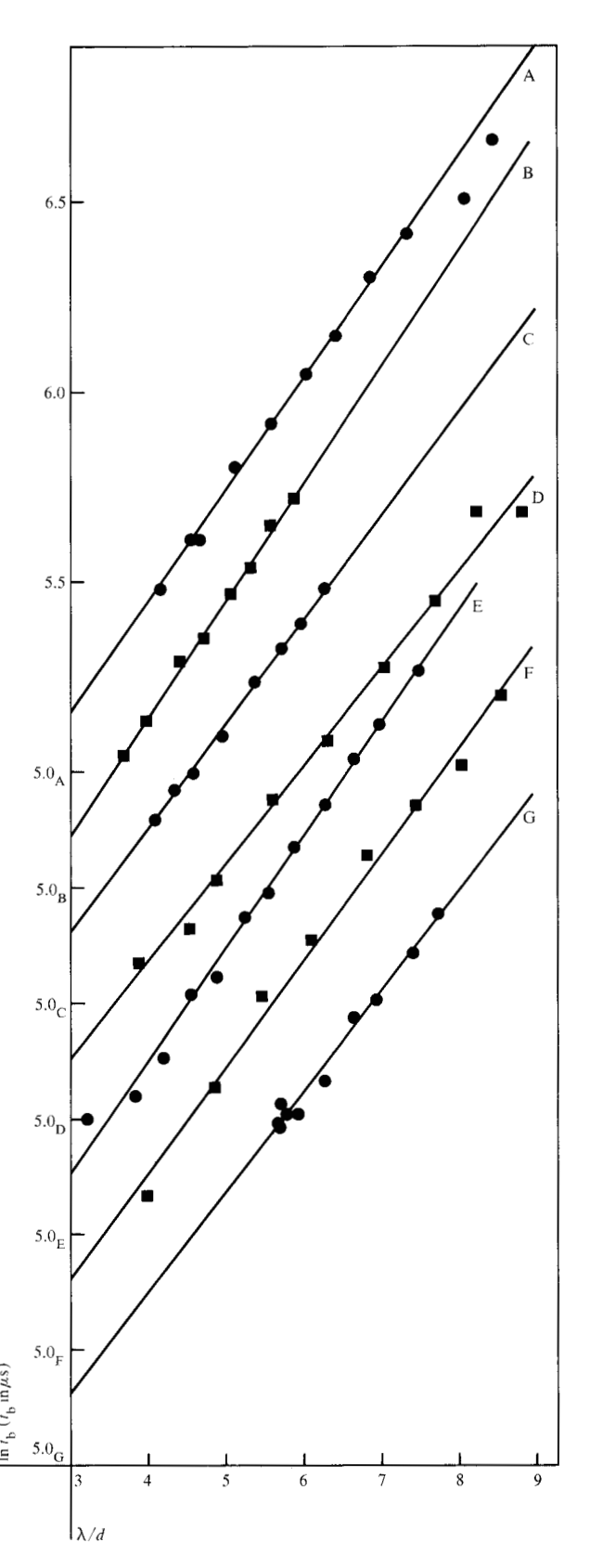


Figure 4 Data derived from observations of the infinite satellite condition. The ordinate scale is shown only for data set A; the other scales are the same but are displaced downward as indicated; see Table 1.

[†]Distilled water.



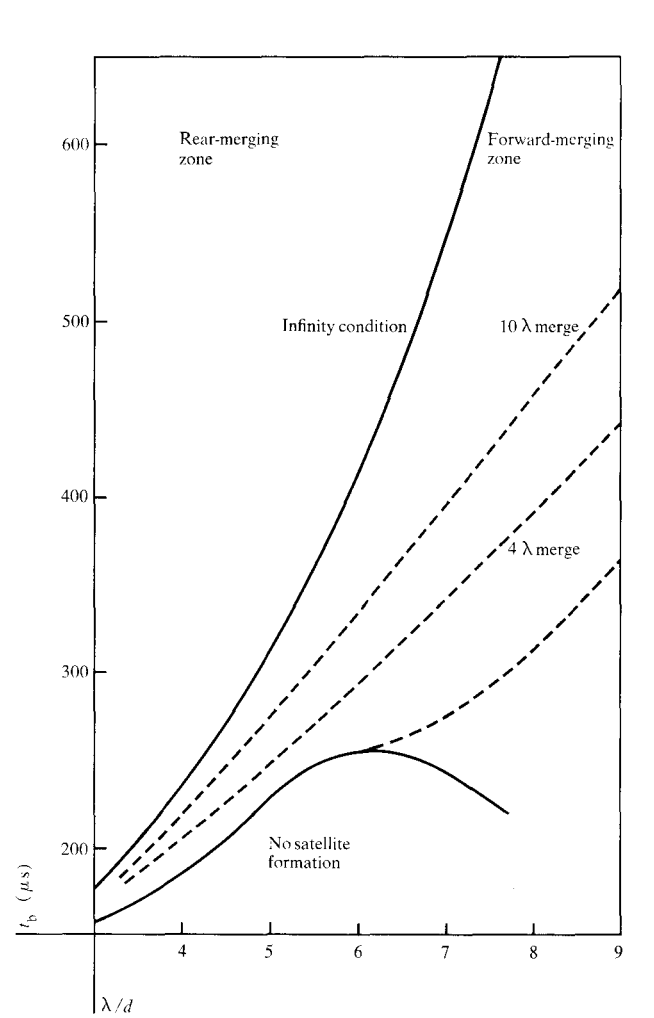


Figure 5 "Map" of the satellite condition.

logarithms of the derived break-off times are plotted against wavelength (interdrop spacing). The slopes and intercepts of these lines are listed in Table 1. Within experimental error, the slopes and intercepts are essentially equal. Thus, for these data, which involved five different mechanical assemblies, different vibration frequencies, and two liquids, one empirical relation seems to suffice:

$$t_{\rm b_{\infty}} = 76 \ e^{0.28\lambda/d}.$$
 (2)

Figure 5 is a plot incorporating all of the data taken. The upper solid curve is the infinity condition as given by Eq. (2). The lower solid curve gives the boundary below which no satellite formation takes place. The "window" for ink jet printing is below this latter curve which, however, is not nearly so well defined by the data as the infinity condition is. A lower bound for the print window is not shown, but we have observed that when the exciting current is increased beyond the region of linear operation, satellite formation again occurs. For larger

currents, the onset of the nonlinear operation of the vibrating head would be indicated by the data departing from the straight-line relationship shown in Fig. 2. For ink jet printing, therefore, one should operate in the linear region.

Extending upward from the peak of the no-satellite boundary is a quasi-boundary for longer wavelengths. Along and below this curve satellite separation does not always occur. In this region either two to four wavelengths are required before the ligament rejoins the parent drop or, ultimately, satellite separation occurs two to four wavelengths downstream from the initial spreading. (These latter semi-quantitative observations pertain to the relatively viscous ink, whereas in distilled water the satellite separation occurs more quickly.)

The other two dashed curves in Fig. 5 show the approximate parameter values at which satellites merge forward at four and at ten wavelengths downstream from their formation. The actual data-scatter around these representative curves is considerable.

The satellite condition depends upon whether the fore or the aft end of the satellite separates first and how much time exists between the two separations. We call this time interval the *satellite interaction time*. It is within this interval that momentum transfer takes place, which results in the slowing down or speeding up of the satellite relative to the rest of the stream. As mentioned previously, no momentum transfer takes place when the satellite separates at both ends simultaneously (the infinite satellite condition).

When the drop formation in a jet is stabilized at the lowest possible excitation, rear-merging satellites are observed. In general, these satellites merge within two to four wavelengths downstream from the separation point. As the excitation amplitude is increased, the distance for merging increases until the infinity condition is reached. Thereafter, forward-merging satellites are observed. As the excitation is further increased, the forward-merging satellites require less distance to merge until the condition is reached in which satellite separation no longer takes place. Beyond this point is thus the desired drop condition, with no satellite formation occurring. Stated somewhat differently, at higher excitation amplitudes the satellite interaction time can increase enough so that the second separation is entirely frustrated, resulting in no actual satellite formation.

The satellite interaction time is dependent on wavelength as well as on excitation level. As can be discerned from Fig. 4, the interaction time increases with increasing wavelength. Thus at shorter wavelengths (from 3.2 to about 4.7 diameters), satellite formation is quite persistent due to inadequate interaction time.

That observation might lead one to expect better drop formation at longer wavelengths. However, at the longer wavelengths (greater interdrop spacing) the satellite droplets tend to be much larger and the ligaments between drops and impending satellites much longer. Therefore, relatively long satellite interaction times become necessary in order to frustrate satellite formation.

We have essentially a maximum-minimum type of problem in that there are two effects, each of which tends to insure complete satellite formation. At shorter wavelengths, an inadequate interaction time does not permit the frustration of satellite formation. At longer wavelengths, larger masses would have to be moved over longer distances in order to frustrate the satellite formation. As it turns out, the range of λ from 5 to 6.5 diameters is the best range for frustrating the formation of satellite droplets.

Spatial instability analysis

The nonlinear differential equations for the one-dimensional problem of drop formation have been presented previously [5-7]:

$$r\frac{\partial v}{\partial z} = -2\left(v\frac{\partial r}{\partial z} + \frac{\partial r}{\partial t}\right),$$

$$\frac{\partial v}{\partial t} + v\frac{\partial v}{\partial z} = -\frac{1}{\rho}\frac{\partial p}{\partial z},$$
(3)

where p, the pressure, is given by

$$p = \frac{T}{\sqrt{1 + (\partial r/\partial z)^2}} \left[\frac{1}{r} - \frac{(\partial^2 r/\partial z^2)}{1 + (\partial r/\partial z)^2} \right]. \tag{4}$$

The dependent variables in these equations are r and v, respectively the radius of the column of liquid and the axial velocity. These variables are dependent on time t and axial displacement z; T is the surface tension of the liquid boundary, and ρ is the density of the liquid.

The solution is to be constrained by the following boundary conditions at z = 0:

$$r = a$$

$$\frac{\partial r}{\partial z} = \frac{\partial^2 r}{\partial z^2} = 0,$$

$$v = v_0 (1 + \nu \cos 2\pi f t), \tag{5}$$

where v_0 is the jet velocity and $\nu \equiv \Delta v/v_0$ is the relative amplitude of the velocity perturbation imposed thereon with frequency f.

For this analysis we make the following substitutions and definitions:

$$r = a(1 + \delta), \quad v = v_0(1 + u),$$

$$t = \frac{a\tau}{v_0}, \qquad z = a\xi$$

$$\omega = \frac{2\pi a}{\lambda}, \qquad \epsilon = \sqrt{\frac{T}{2\alpha a v_{\perp}^2}}. \tag{6}$$

The boundary conditions at $\xi = 0$ become

$$\delta = \frac{\partial \delta}{\partial \xi} = \frac{\partial^2 \delta}{\partial \xi^2} = 0,$$

$$u = v \cos \omega \tau.$$
(7)

The differential equations now take the form

$$(1+\delta)\frac{\partial u}{\partial \xi} = -2\left[(1+u) \frac{\partial \delta}{\partial \xi} + \frac{\partial \delta}{\partial \tau} \right],$$

$$\frac{\partial u}{\partial \tau} + (1+u) \frac{\partial u}{\partial \xi} = -\frac{2 a\epsilon^2}{T} \frac{\partial p}{\partial \xi}.$$
 (8)

If ν is very small, we can use it as an expansion parameter for the solutions δ and u:

$$\delta = \nu \delta_1 + \nu^2 \delta_2 + \nu^3 \delta_3 + \cdots,$$

$$u = \nu u_1 + \nu^2 u_2 + \nu^3 u_3 + \cdots.$$
(9)

Then, through second order,

$$\frac{\partial P}{\partial \xi} = \frac{\nu T}{a} \left(-\frac{\partial \delta_1}{\partial \xi} - \frac{\partial^3 \delta_1}{\partial \xi^3} \right) + \frac{\nu^2 T}{a} \left(-\frac{\partial \delta_2}{\partial \xi} - \frac{\partial^3 \delta_2}{\partial \xi^3} + 2\delta_1 \frac{\partial \delta_1}{\partial \xi} - \frac{\partial \delta_1}{\partial \xi} \frac{\partial^2 \delta_1}{\partial \xi^2} \right). \tag{10}$$

When Eqs. (9) and (10) are substituted into Eq. (8), we have, through second order in ν ,

$$\frac{\partial u_1}{\partial \xi} + 2\left(\frac{\partial \delta_1}{\partial \xi} + \frac{\partial \delta_1}{\partial \tau}\right) = 0,$$

$$\frac{\partial u_1}{\partial \tau} + \frac{\partial u_1}{\partial \xi} - 2\epsilon^2 \left(\frac{\partial \delta_1}{\partial \xi} + \frac{\partial^3 \delta_1}{\partial \xi^3} \right) = 0,$$

$$\frac{\partial u_2}{\partial \mathcal{E}} + 2\left(\frac{\partial \delta_2}{\partial \mathcal{E}} + \frac{\partial \delta_2}{\partial \tau}\right) = F,$$

$$\frac{\partial u_2}{\partial \tau} + \frac{\partial u_2}{\partial \mathcal{E}} - 2\epsilon^2 \left(\frac{\partial \delta_2}{\partial \mathcal{E}} + \frac{\partial^3 \delta_2}{\partial \mathcal{E}^3} \right) = G, \tag{11}$$

where

$$F = -\left(\delta_1 \frac{\partial u_1}{\partial \xi} + 2u_1 \frac{\partial \delta_1}{\partial \xi}\right),$$

$$G = -u_1 \frac{\partial u_1}{\partial \xi} + 2\epsilon^2 \left(\frac{\partial \delta_1}{\partial \xi} \frac{\partial^2 \delta_1}{\partial \xi^2} - 2\delta_1 \frac{\partial \delta_1}{\partial \xi}\right). \tag{12}$$

The solution to the first-order equations, the first two of Eqs. (11), has been given previously [5]. The linear solution, with Eqs. (7) as the boundary conditions, can be given in the form

$$\delta_1 = \sum_{j=1}^4 C_j \kappa_j \cos \Theta_j,$$

$$u_1 = \sum_{j=1}^4 d_j \cos \Theta_j,$$
(13)

where

$$\begin{split} \Theta_{j} &\equiv \omega \tau - \kappa_{j} \xi, \\ C_{j} &\equiv \frac{\frac{1}{4}\omega}{(1 + \epsilon^{2})\kappa_{j}^{2} - 3\omega \kappa_{j} + 2\omega^{2}}, \\ d_{j} &\equiv 2C_{j}(\omega - \kappa_{j}); \\ \kappa_{1} &\equiv \gamma + i\sigma, \\ \kappa_{2} &\equiv \gamma - i\sigma, \\ \kappa_{3} &\equiv -\gamma + \beta, \\ \kappa_{4} &\equiv -\gamma - \beta, \end{split}$$

where γ and β are real constants;

$$\sigma^{2} = \frac{\omega}{2\gamma\epsilon^{2}} + \left(\gamma^{2} - \frac{1+\epsilon^{2}}{2\epsilon^{2}}\right),$$

$$\beta^{2} = \frac{\omega}{2\gamma\epsilon^{2}} - \left(\gamma^{2} - \frac{1+\epsilon^{2}}{2\epsilon^{2}}\right),$$

$$4\epsilon^{4}\gamma^{6} - 2\epsilon^{2}(1+\epsilon^{2})\gamma^{4}$$

$$+ \left[\frac{1}{4}(1+\epsilon^{2})^{2} + \omega^{2}\epsilon^{2}\right]\gamma^{2} - \frac{1}{4}\omega^{2} = 0.$$
(14)

To determine the particular solution of the secondorder equations, the last two of Eqs. (11), the F and G of (12) must be evaluated. Upon substituting the linear solution into (12),

$$\begin{split} F &= \sum_{j=1}^{4} f_{jj} \sin 2\Theta_{j} \\ &+ \sum_{n=-j+1}^{4} \sum_{j=1}^{3} \left[f_{jn} \sin \left(\Theta_{j} + \Theta_{n} \right) + \tilde{f}_{jn} \sin \left(\Theta_{j} - \Theta_{n} \right) \right], \\ G &= \sum_{j=1}^{4} g_{jj} \sin 2\Theta_{j} \\ &+ \sum_{n=-j+1}^{4} \sum_{j=1}^{3} \left[g_{jn} \sin \left(\Theta_{j} + \Theta_{n} \right) + \tilde{g}_{jn} \sin \left(\Theta_{j} - \Theta_{n} \right) \right], \end{split}$$

where

$$\begin{split} f_{jj} &\equiv 3C_{j}^{2}\kappa_{j}^{2}(\kappa_{j}-\omega), \\ f_{jn} &\equiv C_{j}C_{n}[3\kappa_{j}\kappa_{n}(\kappa_{j}+\kappa_{n})-2\omega(\kappa_{j}^{2}+\kappa_{j}\kappa_{n}+\kappa_{n}^{2})], \\ \tilde{f}_{jn} &\equiv C_{j}C_{n}(\kappa_{j}-\kappa_{n})[3\kappa_{j}\kappa_{n}-2(\kappa_{j}+\kappa_{n})], \\ g_{jj} &= -C_{j}^{2}\kappa_{j}[2(\kappa_{j}-\omega)^{2}+\epsilon^{2}\kappa_{j}^{2}(2+\kappa_{j}^{2})], \\ g_{jn} &= -C_{j}C_{n}(\kappa_{j}+\kappa_{n})[2(\kappa_{j}-\omega)(\kappa_{n}-\omega)+\epsilon^{2}\kappa_{j}\kappa_{n}(2+\kappa_{j}\kappa_{n})], \\ \tilde{g}_{jn} &= -C_{j}C_{n}(\kappa_{j}-\kappa_{n})[2(\kappa_{j}-\omega)(\kappa_{n}-\omega)+\epsilon^{2}\kappa_{j}\kappa_{n}(2-\kappa_{j}\kappa_{n})]. \end{split}$$

With F and G as given by (15), the pair of secondorder equations separates into 16 independent equations. The 16 solutions which form the particular solution to the equations can be written as

$$\begin{split} \delta_{\text{2p}} &= \sum_{j=1}^{4} A_{jj} \cos 2\Theta_{j} \\ &+ \sum_{n=1}^{4} \sum_{j=1}^{3} \left[A_{jn} \cos \left(\Theta_{j} + \Theta_{n} \right) \right. \\ &+ \tilde{A}_{jn} \cos \left(\Theta_{j} - \Theta_{n} \right) \right], \\ u_{\text{2p}} &= \sum_{j=1}^{4} B_{jj} \cos 2\Theta_{j} \\ &+ \sum_{n=1}^{4} \sum_{j=1}^{3} \left[B_{jn} \cos \left(\Theta_{j} + \Theta_{n} \right) \right. \\ &+ \tilde{B}_{jn} \cos \left(\Theta_{j} - \Theta_{n} \right) \right]. \end{split}$$
(17)

The 32 constants of Eqs. (17) are obtained by substituting this solution into the differential equations. As a result, the following three sets of equations are used to calculate these constants:

$$\frac{1}{2}f_{jj} = \kappa_{j}B_{jj} + 2(\kappa_{j} - \omega)A_{jj},$$

$$\frac{1}{2}g_{jj} = (\kappa_{j} - \omega)B_{jj} + 2\epsilon^{2}\kappa_{j}[1 - 4\kappa_{j}^{2}]A_{jj};$$

$$f_{jn} = (\kappa_{j} + \kappa_{n})B_{jn} + 2[(\kappa_{j} + \kappa_{n}) - 2\omega]A_{jn},$$

$$g_{jn} = [(\kappa_{j} + \kappa_{n}) - 2\omega]B_{jn}$$

$$+ 2\epsilon^{2}(\kappa_{j} + \kappa_{n})[1 - (\kappa_{j} + \kappa_{n})^{2}]A_{jn};$$

$$\tilde{f}_{jn} = (\kappa_{j} - \kappa_{n})\tilde{B}_{jn} + 2(\kappa_{j} - \kappa_{n})\tilde{A}_{jn},$$

$$\tilde{g}_{jn} = (\kappa_{j} - \kappa_{n})\tilde{B}_{jn}$$

$$- 2\epsilon^{2}(\kappa_{j} - \kappa_{n})[1 - (\kappa_{i} - \kappa_{n})^{2}]\tilde{A}_{jn}.$$
(18)

As with the presentation of the linear solution [5], this second-order solution is presented in complex form. The solution, however, is real; the complex factors and terms exist in conjugate pairs that combine to form a real solution.

The linear portion of the problem already satisfies the boundary conditions. Therefore, the general second-order solution must cancel the values of the particular second-order solution at the boundary. The boundary values for the general solution at $\xi = 0$ are

$$\begin{split} \delta_{2\mu} &= R_1 \cos 2\omega \tau + R_2, \\ \frac{\partial \delta_{2\mu}}{\partial \xi} &= R_3 \sin 2\omega \tau, \\ \frac{\partial^2 \delta_{2\mu}}{\partial \xi^2} &= R_4 \cos 2\omega \tau + R_5, \\ u_{2\mu} &= R_6 \cos 2\omega \tau + R_7, \end{split} \tag{19}$$

26

where the seven real constants are given by

$$R_{1} = -\sum_{j=1}^{4} A_{jj} - \sum_{\substack{n=1\\j+1}}^{4} \sum_{j=1}^{3} A_{jn},$$

$$R_{2} = -\sum_{\substack{j=1\\j+1}}^{4} \sum_{j=1}^{3} \tilde{A}_{jn},$$

$$R_{3} = -\sum_{\substack{j=1\\j+1}}^{4} 2\kappa_{j}A_{jj} - \sum_{\substack{n=1\\j+1}}^{4} \sum_{j=1}^{3} (\kappa_{j} + \kappa_{n})A_{jn},$$

$$R_{4} = \sum_{j=1}^{4} 4\kappa_{j}^{2}A_{jj} + \sum_{\substack{n=1\\j+1}}^{4} \sum_{j=1}^{3} (\kappa_{j} + \kappa_{n})^{2}A_{jn},$$

$$R_{5} = \sum_{\substack{n=1\\j+1}}^{4} \sum_{j=1}^{3} (\kappa_{j} - \kappa_{n})^{2}\tilde{A}_{jn},$$

$$R_{6} = -\sum_{\substack{j=1\\j+1}}^{4} B_{jj} - \sum_{\substack{n=1\\j+1}}^{4} \sum_{j=1}^{3} B_{jn},$$

$$R_{7} = -\sum_{\substack{n=1\\j+1}}^{4} \sum_{j=1}^{3} \tilde{B}_{jn}.$$
(20)

The general second-order solution can be considered in two parts, the time-independent part satisfying the constant terms of the boundary conditions (19) and the other part obeying the time-varying terms of (19). The time-independent part of the solution is

$$\begin{split} \tilde{\delta}_{2g} &= R_2 + \frac{R_5}{k^2} (1 - \cos k\xi), \\ \tilde{u}_{2g} &= R_7 - \frac{2R_5}{k^2} (1 - \cos k\xi), \\ k &\equiv \sqrt{1 + \epsilon^2} / \epsilon. \end{split} \tag{21}$$

The solution to the time-dependent part is analogous to the linear solution presented previously. However, ω must be changed to 2ω and the matrix equation that determines the coefficients becomes more complicated. The solution may be written as

$$\delta_{2\mu} = \sum_{j=1}^{4} \tilde{C}_{j} \tilde{\kappa}_{j} \cos \tilde{\Theta}_{j},$$

$$u_{2g} = \sum_{j=1}^{4} \tilde{d}_{j} \cos \tilde{\Theta}_{j}.$$
(22)

In this solution, $\tilde{\Theta}_j$, \tilde{d}_j , $\tilde{\kappa}_j$, $\tilde{\sigma}$, $\tilde{\beta}$, and $\tilde{\gamma}$ are all defined in a manner analogous to the definitions (14). The only difference is that 2ω replaces ω in those equations. The constants \tilde{C}_j , however, take the following form because of the more complicated boundary conditions:

$$\tilde{C}_{j} = \frac{\omega(R_{6} + 2R_{1}) + \tilde{\kappa}_{j} [\epsilon^{2} \tilde{\kappa}_{j}^{2} - (1 + \epsilon^{2})] R_{1} + \epsilon^{2} \tilde{\kappa}_{j}^{2} R_{3} + \tilde{\kappa}_{j} \epsilon^{2} R_{4}}{2[(1 + \epsilon^{2}) \tilde{\kappa}_{i}^{2} - 6\omega \tilde{\kappa}_{i} + 8\omega^{2}]}$$
(23)

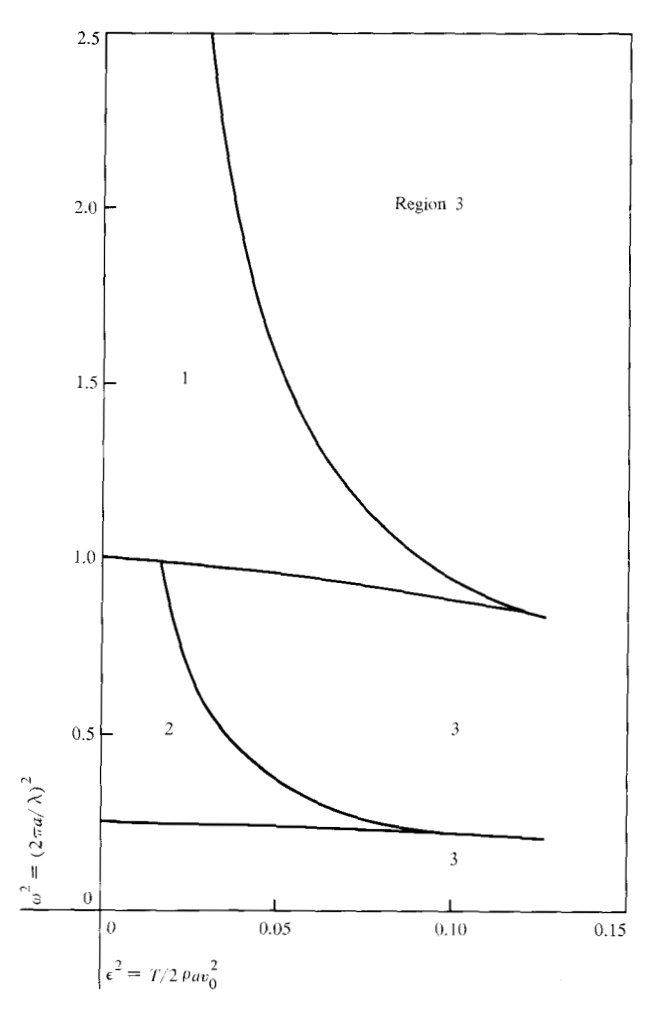


Figure 6 Regions for satellite droplet formation in parameter space.

The total solution to the spatial instability problem may now be written through second order as

$$\begin{split} \delta &= \nu \delta_1 + \nu^2 (\delta_{2p} + \delta_{2g} + \tilde{\delta}_{2g}), \\ u &= \nu u_1 + \nu^2 (u_{2p} + u_{2g} + \tilde{u}_{2g}), \end{split} \tag{24}$$

using appropriate substitutions from (13), (17), (21), and (22).

Discussion

For various values of the parameters ω^2 and ϵ^2 , the solution can grow in an exponential fashion, leading to drop formation and separation. The ranges of these parameters for such formation to occur for the *linear terms* have been discussed previously [5]. In Fig. 6, region 1 shows the range of parameters in which all four of the controlling eigenvalues κ_j are real. Hence, all of the functions are circular; no drop formation takes place. In regions 2 and

3, however, the first two eigenvalues are complex. As a result, hyperbolic functions appear in the solution, and drop growth ensues.

The particular second-order solution, Eq. (17), is controlled by the same four eigenvalues. There is no drop formation in region 1 of Fig. 6, whereas drop formation does proceed in regions 2 and 3.

The general second-order solution, Eqs. (21) and (22), is controlled by a different set of eigenvalues, the $\tilde{\kappa}_j$ and k. All five of these values are real in regions 1 and 2. The first two eigenvalues are complex, however, in region 3. Therefore, in region 1, no drop formation takes place; in region 2, only linear terms and particular second-order terms contribute to drop formation; and it is only in region 3 that terms of the general second-order solution grow in an exponential fashion.

Let us consider the solution at drop separation only for values of ϵ^2 which are much less than one. In this so-called Rayleigh range, which has been discussed previously [5], the jet velocity is significantly greater than the capillary velocity in the jet. The experiments reported in this paper, as well as most of the experimental work reported in the literature, were performed in this range of small ϵ^2 .

Many of the terms in the theoretical solution do not contribute significantly to the answer and can be ignored. In fact, at least for small ϵ^2 , our calculation shows that terms which contain the eigenvalues κ_3 , κ_4 , $\tilde{\kappa}_3$, $\tilde{\kappa}_4$, and k may be neglected. By approximating hyperbolic functions as exponential ones near the drop separation point, one can write

$$\delta = \nu \delta_1 + \nu^2 \delta_{2n} + \nu^2 \delta_{2n} + \cdots, \tag{25}$$

where

$$\nu\delta_{1} \approx -e^{\sigma(\xi-\xi_{b})} \sin(\omega\tau - \gamma\xi),$$

$$\nu^{2}\delta_{2p} \approx -e^{2\sigma(\xi-\xi_{b})} \left[\frac{1}{4} + \frac{(1-2\omega^{2})}{4\omega^{2}} \cos 2(\omega\tau - \gamma\xi) + \frac{\sigma}{\omega^{3}} \sin 2(\omega\tau - \gamma\xi) \right]$$

$$+ \frac{(\omega^{2}-4)}{2(4\omega^{2}-1)} e^{-2\sigma\xi_{b}} \cos 2(\omega\tau - \gamma\xi),$$

$$\nu^{2}\delta_{2g} \approx e^{-2\sigma\xi} \left[4\omega P \cos |\tilde{\sigma}|\xi \cos (2\omega\tau - \tilde{\gamma}\xi) + 2(\tilde{\sigma}P + 2\omega Q) \sin |\tilde{\sigma}|\xi \sin (2\omega\tau - \tilde{\gamma}\xi) \right];$$

$$P \equiv \frac{9\omega^{4} - 10\omega^{2} + 1}{8\omega^{3}(1 - 4\omega^{2})},$$

$$Q \equiv \frac{\epsilon^{2}}{|\tilde{\sigma}|} \frac{14\omega^{6} - 32\omega^{4} + 21\omega^{2} - 3}{4\omega^{2}(4\omega^{2} - 1)},$$
(26)

and σ is defined in Eqs. (14). In these equations, ξ_b is the separation distance predicted by the linear theory [5]:

$$e^{-\sigma\xi_{\mathbf{b}}} = \omega\nu/4\sigma. \tag{27}$$

The terms from the general solution in Eqs. (26) are given in a form that is valid for region 2 where these terms do not grow exponentially. In region 3, a different form that includes hyperbolic functions is required.

Calculations from the second-order spatial instability analysis show satellite droplet formation for perturbation wavelengths greater than about 5.5 jet diameters. For shorter wavelengths, and for small perturbation amplitudes and small values of ϵ^2 , no satellite formation is predicted. This conflicts with experimental evidence, which shows that persistent satellite formation exists at shorter wavelengths. This same situation exists in a second-order temporal instability analysis, developed in a similar way, wherein the second-order solution predicts a wavelength boundary at about 5.4 diameters, below which satellites will not form, whereas the complete nonlinear solution, as presented by Lee [7], shows satellite formation for all wavelengths. Clearly, the higher order terms are required to give a complete picture of satellite droplet formation.

A look at the exponential factors in Eqs. (26) shows that, for both the first- and the second-order solutions, these factors grow to the order of one as drop separation occurs. From the form of the analysis, it can be seen that higher order terms also exist, which approach the order of one at drop separation. These higher order terms can, therefore, contribute significantly to the complete solution.

Figure 7 shows the effect of perturbation amplitude on the drop formation. For a perturbation wavelength of six diameters and for $\epsilon^2 = 0.002$, these drop formation shapes in the vicinity of the separation point were calculated from the first of Eqs. (24). This "pinching" of the jet column shows the same shape tendencies as are observed experimentally. For small perturbations (long break-off distances ξ_b) the first separation occurs on the fore side of the satellite; a slightly lower satellite velocity and rearmerging result. For a single critical perturbation amplitude corresponding to $\xi_b = 90$, the satellite separates at both ends simultaneously, which is the infinite satellite condition. At higher excitation amplitudes (shorter break-off distances), forward-merging satellites are formed.

The second-order theory predicts the infinite satellite condition for a break-off length $\xi_b = 90$. The empirical relation (2) gives a corresponding value of $\xi = 185$ when ϵ^2 is set equal to 0.002. It can be seen, therefore, that the second-order theory gives a good qualitative description of the effect.

In the Appendix of Ref. 5, the slowing down of the jet during drop formation was predicted using gross momentum considerations. This phenomenon is not predicted by linear analyses. A time-independent term in Eq. (17) brings in this effect:

$$\nu^2 \tilde{B}_{12} \cos (\Theta_1 - \Theta_2) \approx \frac{1}{2} \epsilon^2 (3\omega^2 - 5) e^{2\sigma(\xi - \xi_b)},$$
 (28)

where the approximation is for small ϵ^2 . At the separation point,

$$v = v_0 [1 - \epsilon^2 (\frac{5}{2} - \frac{3}{2}\omega^2)]. \tag{29}$$

Previously [5], we obtained the more accurate expression $v = v_0(1 - \epsilon^2)$. Again, it can be seen that our second-order theory describes the effect qualitatively, although the complete nonlinear equations are needed to develop quantitative accuracy.

Summary

A liquid jet, breaking up into drops, tends to form satellite droplets interspersed among the main drops of the stream. Depending upon various conditions, satellite separation can occur on the fore side of the droplet first, on the aft side first, or at both ends simultaneously.

The satellite interaction time, defined as the time between the break-offs of the two ends of a satellite, allows a momentum transfer between the satellite droplet and a main drop of the stream. This transfer alters the velocity of the satellite so that it merges with a main drop: Satellite separation occurring first on the fore side of the droplet results in rear-merging satellites; separation first on the aft side causes a forward-merging situation.

The two most relevant parameters that control satellite droplet formation are the amplitude of the perturbation and the wavelength-to-diameter ratio of this perturbation. Very small perturbation amplitudes result in rear-merging satellites. At a higher value of this amplitude the infinity condition occurs; i.e., both ends of the droplet separate simultaneously. As the amplitude is increased above this value, forward-merging occurs and the satellite interaction time also increases.

An investigation of the infinity condition has revealed a relation between perturbation amplitude and wavelength as shown by Eq. (2) and Fig. 4. Shorter wavelengths require a stronger perturbation to cause this condition. For the forward-merging satellite condition [perturbation amplitudes greater than given by Eq. (2)], larger perturbation amplitudes are required at the shorter wavelengths to produce equal satellite interaction times.

For wavelengths of about five to seven jet diameters, the satellite interaction time can become large enough to frustrate the second droplet separation, and no satellite formation results. At shorter wavelengths, the requisite interaction times are more difficult to achieve. At longer wavelengths, the larger droplet volumes and longer ligaments work against the frustration of the second droplet separation; i.e., they make separation more likely.

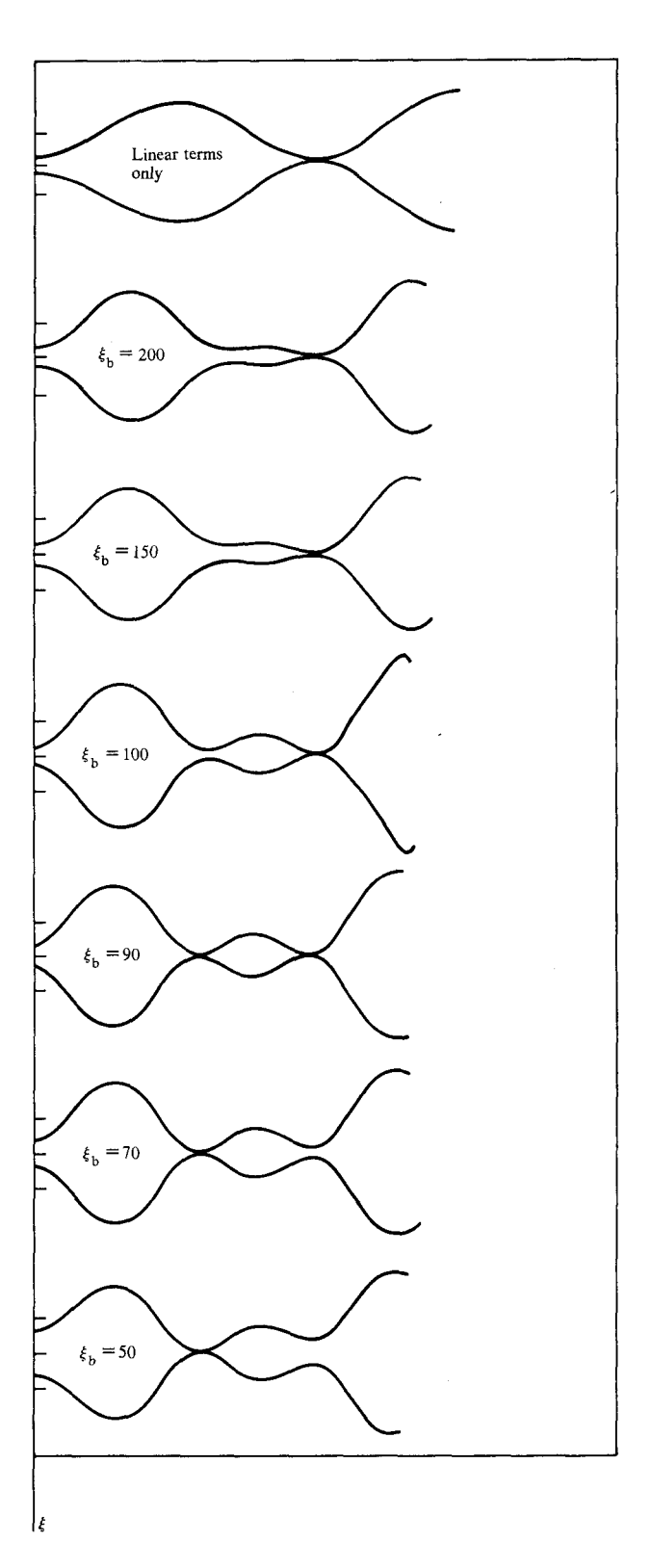


Figure 7 Theoretical drop formation shapes near the separation point. Plotted symmetrically in the vertical direction are the jet column radii r(z) or $r(\xi)$ at an instant of time. The effect of excitation amplitude is shown through the parameter ξ_b ; $\lambda/d=6$ and $\epsilon^2=0.002$.

Linear theories and theories using temporal instabilities are inadequate to describe satellite droplet formation; a nonlinear spatial instability analysis is required. The second-order analysis made in this paper gives a qualitative description of the process. For an accurate quantitative description, the inclusion of higher order terms, or the complete solution of the nonlinear equations, is needed.

In this paper, the jet excitation was purely sinusoidal. It is known, however, that the use of combinations of frequencies or harmonics in the excitation influences satellite droplet formation. The nonlinear spatial instability analysis could be used as a powerful tool to investigate this influence. In addition, the analysis could be used to predict the best combinations of exciting frequencies for use in a particular application.

References

- J. W. S. Rayleigh, "On the Instability of Jets," Proc. London Math. Soc. 10, 4 (1878).
- 2. J. W. S. Rayleigh, *Scientific Papers*, Vol. 1, Cambridge University Press, London, 1899, p. 361.

- C. Weber, "Zum Zerfall eines Flussigkeitsstrahles," Zeitschrift für Angewandte Mathematik und Mechanik 11, 136 (1931).
- 4. J. B. Keller, S. I. Rubinow, and Y. O. Tu, "Spatial Instability of a Jet," *Physics of Fluids* 16, 2052 (1973).
- W. T. Pimbley, "Drop Formation from a Liquid Jet: A Linear One-dimensional Analysis Considered as a Boundary Value Problem," IBM J. Res. Develop. 20, 148 (1976).
- 6. M. C. Yuen, "Non-Linear Capillary Instability of a Liquid Jet," *J. Fluid Mech.* 33, 151 (1968).
- 7. H. C. Lee, "Drop Formation in a Liquid Jet," *IBM J. Res. Develop.* **18**, 364 (1974).

Received May 26, 1976

The authors are located at the IBM System Communications Division laboratory, P.O. Box 6, Endicott, New York 13760.